**Jurnal Penelitian Fisika dan Aplikasinya (JPFA)**
*Volume 13, Issue 02, December 2023*
https://journal.unesa.ac.id/index.php/jpfa/

p-ISSN: 2087-9946
e-ISSN: 2477-1775

# High Preferred Orientation on c-axis of ZnO:GO Crystal Film Synthesized Under Electric Field

**Annisa Nur Rahmawati [1,a], Nabilah Putri Utami [1,b], Lusi Safriani [2,c], Ayi Bahtiar [2,d], Wa Ode Sukmawati Arsyad [3,e], Euis Siti Nurazizah [1,f], and Annisa Aprilia [2,g,*]**

[1] Magister Physics Study Program, Faculty of Mathematics and Natural Sciences, Universitas Padjadjaran
Jl. Raya Bandung-Sumedang KM21, Sumedang 45633, Indonesia
[2] Physics Departement, Faculty of Mathematics and Natural Sciences, Universitas Padjadjaran
Jl. Raya Bandung-Sumedang KM21, Sumedang 45633, Indonesia
[3] Physics Department, Faculty of Mathematics and Natural Sciences, Universitas Halu Oleo
Jl. H.E.A. Mokodompit, Anduonou Kendari 93232, Indonesia

e-mail: [a] annisa17015@mail.unpad.ac.id, [b] nabilah17005@mail.unpad.ac.id, [c] lusi.safriani@phys.unpad.ac.id, [d] ayi.bahtiar@phys.unpad.ac.id, [e] wdsukmawati@uho.ac.id, and [f] euis12001@mail.unpad.ac.id, and [g] a.aprilia@phys.unpad.ac.id
* Corresponding Author

*Received: 3 Oktober 2023; Revised: 19 November 2023; Accepted: 28 December 2023*

***Abstract***

*ZnO nanostructures show a wide range of applications as active materials in optoelectronic devices. The unique structures in 1-dimensional (1D) in combination with other potential materials (such as graphene-based) can increase several device performances. This research aims to observe the influence of an additional electric field (induced by different voltages of ±1 kV) during the growing process of the zinc oxide (ZnO): graphene oxide (GO) crystal. The ZnO:GO layers were prepared via the self-assembly method in 2 steps; the first was seed layer preparation by dip coating technique using $Zn(CH_3COO)_2.2H2O$ and 0.5 (wt%) of $AlCl_3$ as precursor and dopant, respectively. Secondly, growing ZnO rods using $Zn(NO_3)_2{\cdot}6H2O$ as precursor, 0.5 (wt%) GO (dispersed in water) as dopant materials, and hexamethylenetetramine (HMTA) as complexing agent. Applying an external field during self-assembly accelerated the ZnO hexagonal wurtzite crystal formation in a vertical growth direction, increasing the aspect ratio (L/d) of ZnO:GO rods. The direction of the applied external field affected the structure and morphology of the ZnO rods, which relates to ions and seed layer surface polarity during the synthesis process. The addition of an external field during the growing process induced the orderly alignment of ZnO rods, controlling growth perpendicular to the basal plane. This research has a significant scientific impact, elucidating the methods to control the 1D morphology of the ZnO growing process, which is closely related to the surface polarity properties of a material.*

**Keywords:** *ZnO submicron-rods; graphene oxide (GO); self-assembly; external electric field; c-axis preferred orientation*

**How to cite:** Annisa N R, et al. High Preferred Orientation on The c-axis of ZnO:GO Crystal Film Synthesized Under Electric Field. *Jurnal Penelitian Fisika dan Aplikasinya (JPFA)*. 2023; 13(2): 146-159.

DOI: 10.26740/jpfa.v13n2.146-159

## INTRODUCTION

Zinc oxide (ZnO) is a semiconductor material with interesting properties, making it widely studied in materials science, physics, chemistry, biochemistry, and various other sciences [1]. ZnO has a wide band gap (3.37 eV), is transparent in the visible wavelength, and has a large exciton binding energy (60 meV) [2]. ZnO is an abundant natural material with some advantages such as low cost in production, chemically stable in the air, and biologically safe. Zinc oxide can be formed into various nanostructures, one of which is a one-dimensional structure such as nanowires and nanorods. As a functional material in several optoelectronic devices, ZnO, with the modification of nanostructures and combination with other materials, shows an essential aspect in increasing device performance [3]. The improvement in photon conversion efficiency (PCE) of photovoltaic solar cells has been widely reported [4]. Electron transfer in ZnO nanorod crystal occurs much faster, leading to a high electron diffusion coefficient. Zhou et al. reported that the existence of a ZnO nanorod array in a polymer-based photodetector could effectively transfer photogenerated electrons, leading to inhibition in electron-hole pair recombination [5]. ZnO's electrical properties (i.e., charge carrier mobility and conductivity) are strongly related to the morphology and crystallite phase [6].

ZnO's most common crystallographic phase is the hexagonal wurtzite structure in which the $Zn^{2+}$ cations are surrounded by four $O^{2-}$ anions and vice versa [7]. Under standard temperature and pressure conditions, ZnO will crystallize into a wurtzite structure with a space of P63mc (or C6v) and a point group of 6 mm [8]. The wurtzite structure is formed by alternating piles of positively and negatively charged fields consisting of zinc and oxygen atoms, respectively, on the <0001> plane as a basal plane in the direction along the c-axis [9]. The lattice parameters in the ZnO hexagonal wurtzite structure are a and c, equal to 3.2495 Å and 5.2062 Å [10]. Wurtzite ZnO crystal has an electrical polarity, and its polarization is categorized as induced polarization, such as piezoelectric interaction of spontaneous polarization. Piezoelectric polarization occurs due to external strain, which causes the piezoelectric crystal to have macroscopic polarization due to ion transfer. ZnO also tends to have an innate spontaneous polarization along the growth axis (c-axis) [11]. The hexagonal ZnO nanorods exhibit electric dipolar moments along the c-axis and six non-polar m-plane sidewalls in the [1100] direction with relatively low free surface energies.

There are many various ways to modify the structure and morphology of ZnO, one of which is by incorporating other materials such as metal dopants [12], different types of metal oxides [13], or even with an addition of different kinds of material such as carbon-based materials [14]. An addition of carbon-based material such as graphene and its derivatives has been extensively reported [15]. Incorporation of graphene oxide (GO) significantly increases the effectiveness of ZnO photocatalytic activity [16]. GO is derived from a graphite oxide monolayer containing oxygen groups such as epoxy, hydroxyl, carbonyl, etc. [17]. The existence of these oxygen groups can provide excellent dispersibility in water solutions. Other ways of structure and morphology modification are the engineering in the synthesis and preparation process, such as controlling the air and pressure, annealing treatment, precursor concentration, and fabrication technique. There are many routes for manufacturing the ZnO one-dimensional structure. The simplest one is the solution-based synthesis route [18]. ZnO crystals can grow

with uniform size and orientation on the c-axis due to the hexagonal wurtzite structure of ZnO. ZnO naturally consists of polar layers with different charges and causes the growth of the reaction of ZnO crystals aligned by adjusting the growth conditions such as temperature and deposition rate [19]. The chemical environment (i.e., acidity/alkalinity) in the growth solution also influences the formation of ZnO crystal structure [20]. Therefore, this research studied the addition of GO with an alkaline-based solution and the application of an external electric field during the synthesis process. Adding other elements as dopant compounds and applying the electric fields were observed to determine their effect on morphology and crystal growth.

## METHOD

The ZnO:GO layers were prepared in several steps. The first step was the preparation of ZnO:Al as a seed layer using the sol-gel method via dip-coating technique. The ZnO seed layer synthesis was followed by our previous research with a difference in the deposition technique [21]. The materials used were Zinc acetate dihydrate 0.5 M of $Zn(CH_3COO)_2.2H_2O$ as a precursor, Methoxyethanol as a solvent, 0.5 wt.% of aluminum chloride ($AlCl_3$) as dopant, and 2.5 mL of Diethanolamine (DEA) as stabilizer/ligand. A cleaned glass substrate was prepared and immersed in the seed layer solution by dip coating technique with a withdrawal speed of 3.51 mm/s. The seed layer deposition was interspersed with two steps: annealing treatment at 75°C for one minute and at 250°C for 10 minutes. Afterward, the calcination of the seed layer was conducted up to 500°C for 30 minutes at the hotplate. The next step was the synthesis of ZnO and ZnO:GO using the self-assembly method with the addition of an external electric field (induced by ±1 kV). The preparation of growth solution was provided by dissolving 1.17 gram of Zinc nitrate hexahydrate $Zn(NO_3)_2.6H_2O$, Aldrich, 98%) and 0.5 gram hexamethylenetetramine (HMTA, Aldrich, 99%) in 70 mL of deionized (DI) water. 0.5 wt% of GO (4mg/ml) dispersed in water was added to the solution growth. The seed layer, which had been prepared previously, was immersed 45° face down in the growth solution.

Applying an electric field during the deposition process was carried out with two positions of field direction. This scheme aimed to observe the differences in the samples in morphology, structure, and surface properties. The parallel copper plates were set connected to a DC power supply, and placed on the top and bottom of the substrate. The formation of the ZnO hexagonal base grown near the negative pole directed the crystal growth towards the c-axis. The schematic procedure of the applied external field during preparation is shown in Figure 1. The temperature of the heating band was kept at 100°C during self-assembly deposition for 150 minutes.

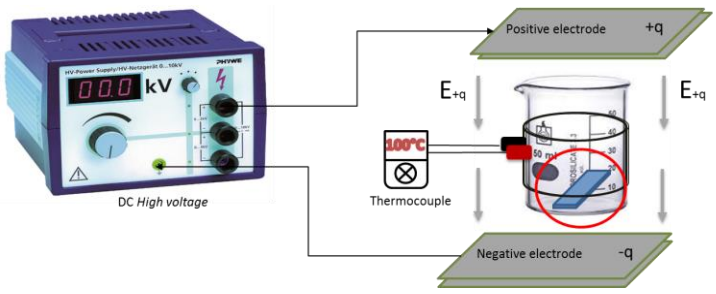


**Figure 1.** Schematic Procedure of ZnO:GO Rod Growth Under External Electric Field

## RESULTS AND DISCUSSION

The mass of each sample was weighed to determine its weight mass and the results are

tabulated in Table 1. The addition of GO enhances the mass of samples. Since dispersed graphene oxide was an alkaline solution with a pH range of 7-11 [22], the enhancement of the sample mass was predicted to be caused by GO, which provides more oxygen and hydroxyl to the system. ZnO naturally consisted of polar layers with different charges. The $Zn^-$ and $O^-$polar surfaces will adsorb $OH^-$ hydroxyl groups and $H^+$ ions in the vicinity, thus enhancing the resulting compound product. The negative electric field configuration (-1 kV) seemed to minimize their free energy formation and an electrical double layer on the surface occurred [11]. ZnO:Al seed layer was estimated to consist in the form of oxygen termination at the surface. The negative electric field configuration supported the cations ($Zn^{2+}$) or $(ZnOH)^+$ to move toward and aggregated to ZnO formation on the seed layer. The opposite situation, when +1kV voltage was applied, hampers the cation's mobility inside the system. The schematic representative of ZnO rod growth is depicted in Figure 2.

**Table 1.** Mass of Each Sample that Resulted from This Research

| Sample | Mass (gram) |
|---|---|
| ZnO | 10 |
| ZnO:GO | 16.7 |
| ZnO:GO (1kV) | 11.3 |
| ZnO:GO (-1kV) | 12.7 |

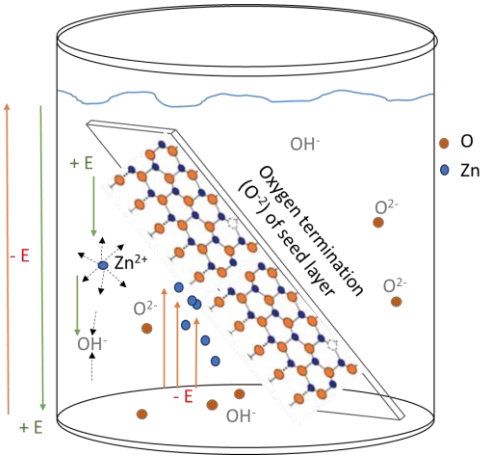


**Figure 2.** The Schematic of ZnO Rod Growth under an External Electric Filed

**Morphological Properties**

Figure 3 shows the SEM images for all samples on the surface and cross section. ZnO morphology from all samples had a length ($L$) and diameter ($d$) that were micron-sized and grew vertically hexagonal. A difference in aspect ratio ($L/d$) was observed as an addition of GO and an electric field applied. Adding GO and an external electric field seemed to accelerate the diameter growth and increase the ZnO mass. Figures 3(a-d) show the surface and cross-section of ZnO and ZnO:GO, which grow without an electric field. The rod size of ZnO:GO was larger than that of ZnO. The increasing rod sizes also induced the hexagonal structure growth to incline each other to produce disordered rod arrays. When +1 kV voltage was applied to the system, the rods' length increased while the diameter decreased. A reduction in average rod diameter was observed when -1 kV voltage was applied. Molefe et al. stated that with many anions in the growth solution (such as $OH^-$ and $O^{2-}$), $Zn^{2+}$ would react, forming a new ZnO

specimen. Conversely, when the anions were limited (or the movement was hampered), $Zn^{2+}$ tended to react with the former ZnO specimen, increasing ZnO particle size [23]. Therefore, the positive electric field seemed to inhibit the $Zn^{2+}$ movement, producing ZnO rods with larger diameters. Meanwhile, the negative electric field kept the anions steady and accelerate $Zn^{2+}$ toward the seed layer, constructing a new ZnO rod specimen. Since the cations easily transferred to the seed layer surface on the substrate, a denser and smaller rod diameter was produced. The ratio between length and diameter (aspect ratio ($L/d$)) of each sample is tabulated in Table 2.

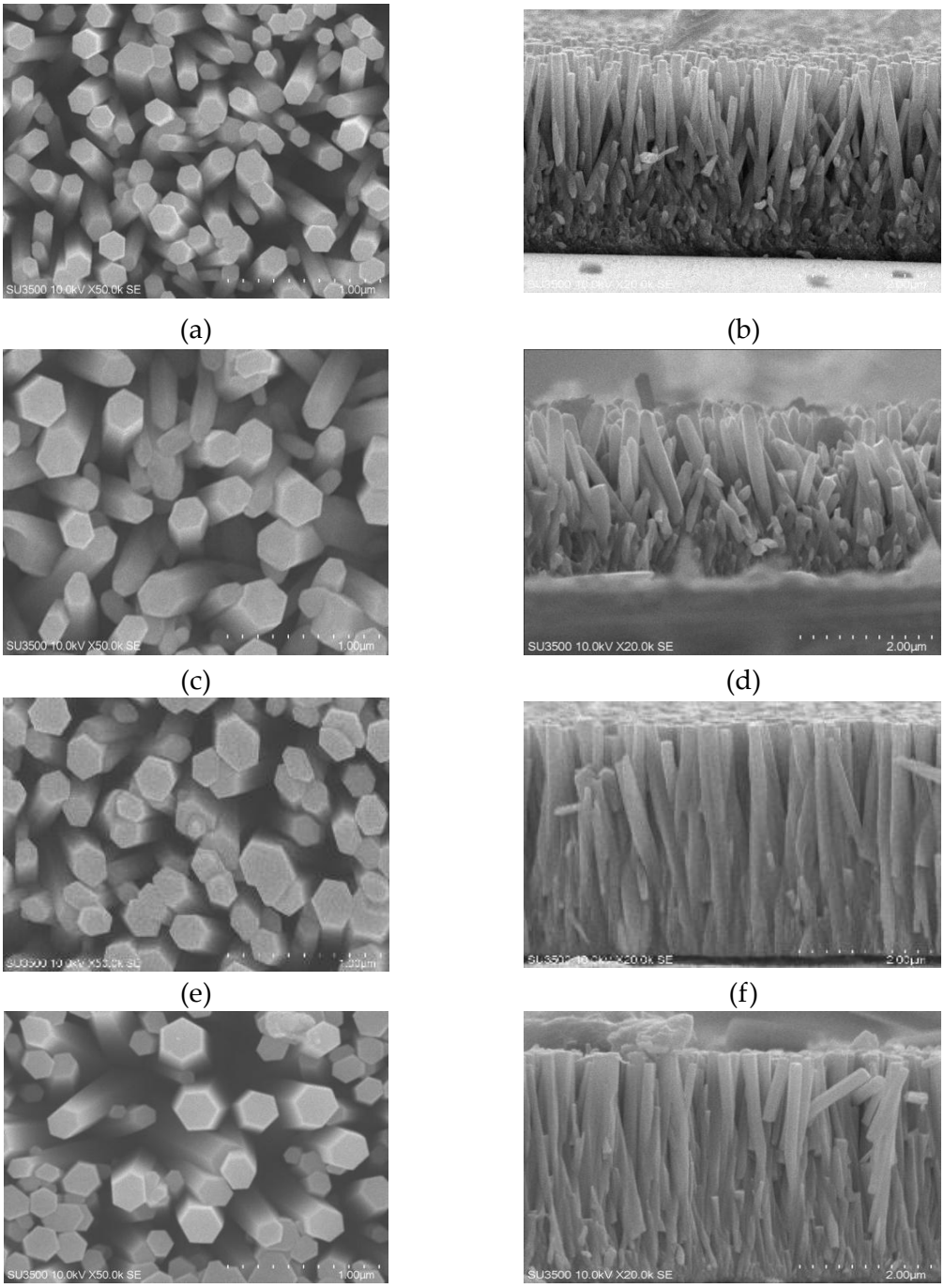


(a) (b) (c) (d) (e) (f) (g) (h)

**Figure 3.** Surface and Cross-Section Morphology of (a)-(b) ZnO, (c)-(d) ZnO:GO, (e)-(f) ZnO:GO 1 kV (+), and (g)-(h) ZnO:GO 1 kV (-)

**Table 1.** Aspect Ratio (L/d) of the Samples

| Sample | Diameter | Length | Aspect Ratio |
|---|---|---|---|

| | d (nm) | L (μm) | (L/d) |
|---|---|---|---|
| ZnO | 180 | 2.50 | 13.89 |
| ZnO:GO | 227 | 2.50 | 11.01 |
| ZnO:GO 1 kV | 217 | 3.25 | 14.97 |
| ZnO:GO - 1 kV | 208 | 3.5 | 15.62 |

EDS characterization was used to determine the element content on ZnO:GO surfaces. The ratio between Zn and O was 1: 0.82, which predicted that some native defects, such as Zn interstitial or O vacancy, were present in the sample. A non-stochiometric between Zn and O atoms on the ZnO:GO surface could also be related to the Zn termination on the surface layer. Atomic % of C element in the surface sample was not detected. The C atoms were probably attached to the cross-section of the ZnO prismatic plane. To confirm the existence of GO on the ZnO sample, Raman spectroscopy was carried out to identify the G-band and D-band characteristics that were specifically present in graphene oxide molecules [24].

**Structure Properties**

The Raman shift spectrum for ZnO:GO that grows under an electric field induced by ±1 kV is shown in Figure 4. The active Raman vibrational mode in the ZnO nanorods represented the hexagonal wurtzite structure. Based on Figure 4, the observed peaks at 100.44 $cm^{-1}$ and 436.46 $cm^{-1}$ of the ZnO:GO 1 kV sample were related to the optical mode E2 (LOW) – zinc sublattice vibration and optical mode E2 (HIGH) – oxygen sublattice vibrations, respectively [25]. The peak of optical mode E2 (LOW) for ZnO:GO (-1 kV) was affected by the interstitial Zn ($Zn_i$), which was identified at 82.30 $cm^{-1}$ [26]. Another oxygen bond O-C-O symmetry that showed a peak of 610.21 $cm^{-1}$ was generated by an oxygen vacancy defect [27]. The presence of peaks 1348.33 $cm^{-1}$and 1596.35 $cm^{-1}$ at ZnO:GO 1 kV (-) and 1349.20 and 1599.31 at ZnO:GO 1 kV (+) indicated the presence of Graphene Oxide compounds in these samples. The GO compound was indicated by the presence of a characteristic D (disorder) band and G (graphite) band, which proved the existence of GO in the samples.

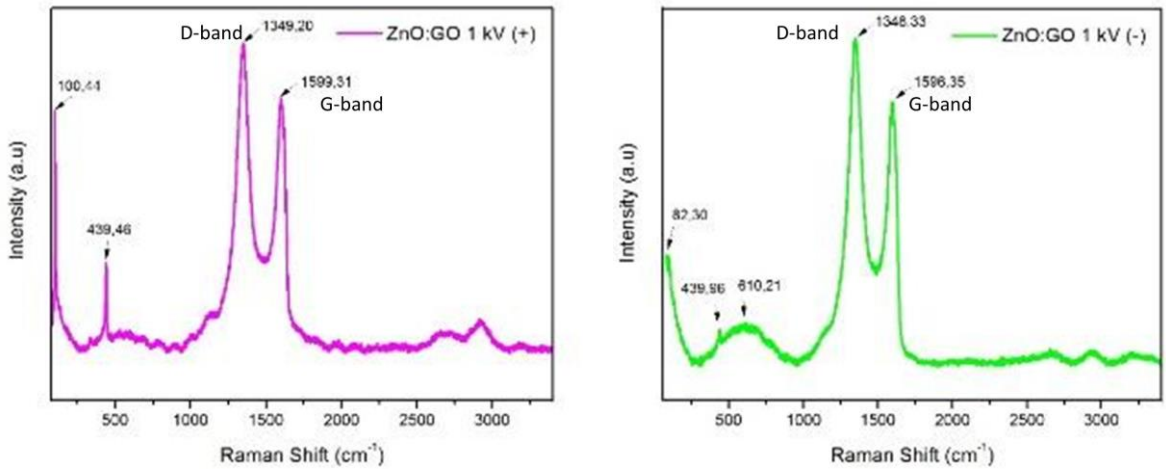


(a) (b)

**Figure 4.** The Results of ZnO Submicron-Rods Sample Measurement using Raman on the Positive and Negative Configuration Samples ZnO:GO 1 kV(+) and ZnO:GO 1 kV(-)

The G bands located at 1599.31 $cm^{-1}$ and 1596.31 $cm^{-1}$ represented the relative degree of graphitization, which established the first-order dispersion of the double-degenerate $E_{2g}$ phonic

mode in the center of the Brillouin zone of $sp^2$-bonded carbon atoms [28]. The D band located at 1349.20 $cm^{-1}$ and 1348.33 $cm^{-1}$ was wider and had a higher intensity than the G band. This finding defined defects in the structure and disturbances induced by the vibrational mode of symmetry $A_{1g}$. The D/G intensity value was 0.84 for the ZnO:GO 1 kV (+) and ZnO:GO 1 kV (-) samples. The electric field induction during the growing process did not significantly affect the existence of GO on the samples.

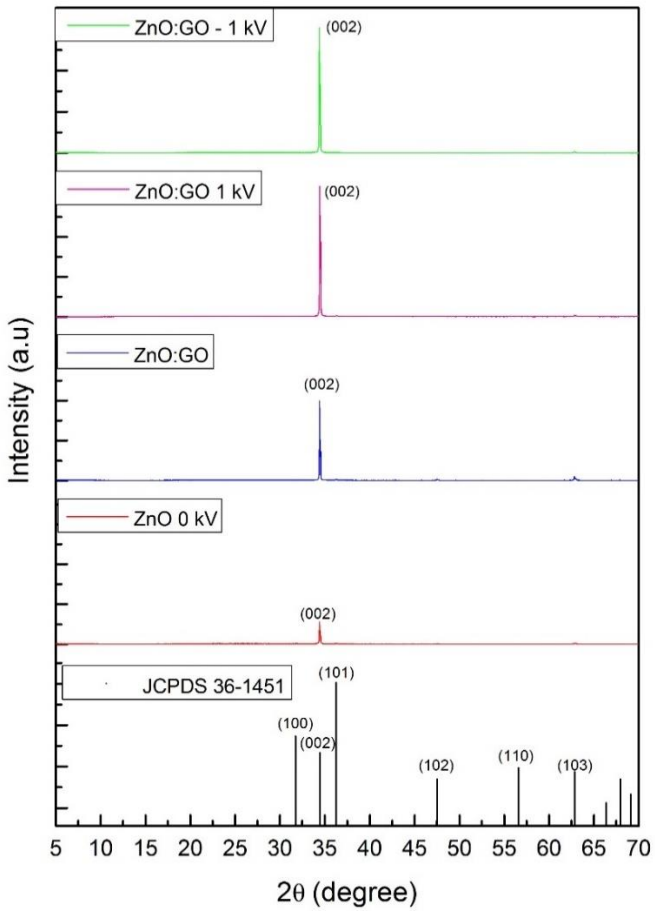


**Figure 5.** XRD Pattern of ZnO and ZnO:GO

XRD characterization was used to determine the crystal structure of the layer by observing the diffraction peaks and Miller's index of the sample. The spectrum for all samples is shown in Figure 5. All samples showed a dominant peak identified as the (002) plane, which showed a highly preferred orientation on the c-axis. This peak is in accordance with JCPDS card No. 36-1451 of ZnO hexagonal wurtzite. In fact, if the spectrum is enlarged (Figure 6), the peak is split becomes two, indicating a different distribution in crystallite size in each sample. The crystallite size of ZnO submicron-rods was calculated using Debye-Scherrer as shown in equation 1 [29]. D is the crystallite size, K is the Scherrer constant (0.9), $\lambda$ is X-ray wavelength (1.54 Å), and $\beta$ denotes the full width at half maximum (FWHM) [30].

$$D = \frac{K\,\lambda}{\beta_{hkl} cos\,\theta} \quad (1)$$

Lorentzian fitting equation was used for spectrum deconvolution to determine the precise FWHM from each split spectrum. The degree of crystallinity (DOC) was calculated by

comparing the peak area of the crystalline phase ($A_c$) with the total peak area that summation of the amorphous phase ($A_a$) and crystalline phase ($A_c + A_a$). The detailed DOC calculation for ZnO:GO 1kV is shown in Figure 7 with the supplied equation. The area of diffraction pattern with yellow shade is identified as the crystallite phase; meanwhile, the grayscale shade is related to the amorphous phase. To understand the effect of an external electric field during the growth process on the ZnO:GO structure, several physical parameters extracted from the XRD pattern were calculated and listed in Table 3.

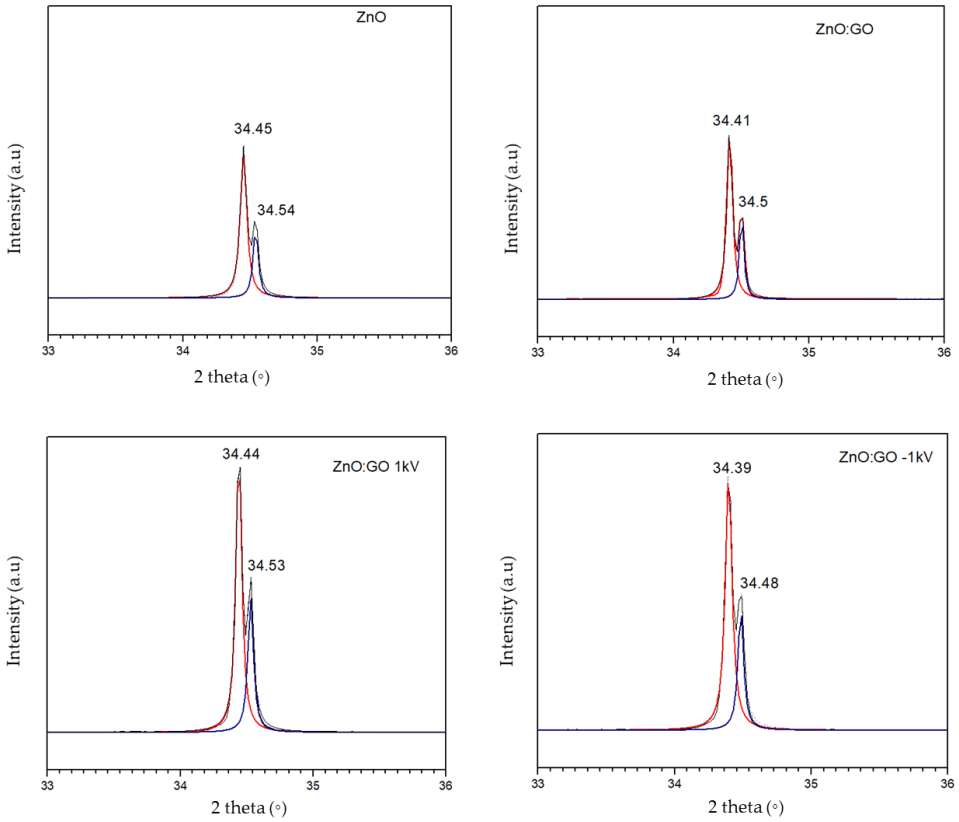


**Figure 6.** Enlarged Spectrum and Its Deconvolution of (002) Plane from the Samples

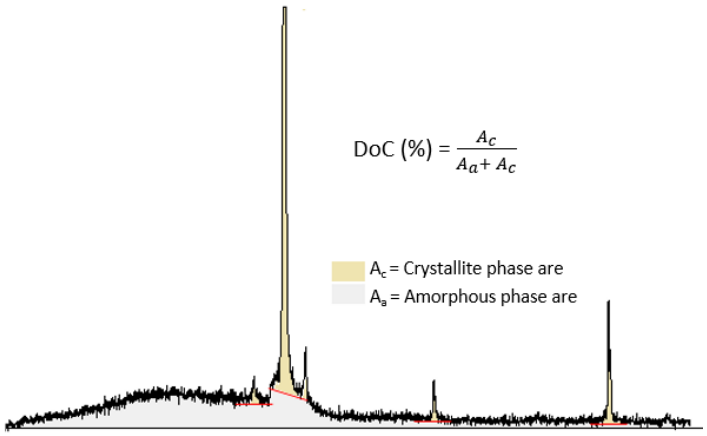


**Figure 7**. The Illustration in Determining of Crystallite and Amorphous Phase from XRD-Pattern

In general, the addition of GO and electric field increased the peak intensity on the XRD spectrum. The FWHM (full-width half maximum) was reduced, indicating the increment in the

average crystallite size of the (002) plane. Based on DOC calculation, the positive of an electric field during the growth process induced the increment amorphous phase, indicating that the faster growth convinced the disordered arrangement of ZnO molecules. SEM images also supported this, which showed an imperfect hexagonal cross-section (Figure 3e). The XRD pattern of ZnO:GO 1 kV shows other slight peaks in (102) and (103) planes. ZnO:GO 1 kV sample had the lowest DOC value but a high rod length. This result indicated that the presence of a positive electric field would decrease the crystallinity due to accelerating ZnO growth. The largest DOC was obtained by sample with the addition of GO without an electric field. Besides the presence of additional oxygen and OH groups from the GO compound, the ZnO formation naturally occurred since ZnO alongside (c-axis) had a minimum surface energy formation [31]. The formation of ZnO crystals without an electric field minimized the defect states and amorphous phases in the ZnO structure but produced an irregular rod arrangement.

**Table 3.** Physical Parameters Determined from XRD Pattern

| Sample | (hkl) | 2θ | FWHM (◦) | B (rad) | D (nm) | $d_{hkl}$ (Å) | c (Å) | *a* (Å) | $\delta$ (×10$^{-5}$ nm$^{-2}$) | DOC |
|---|---|---|---|---|---|---|---|---|---|---|
| ZnO 0 kV | (002) | 34.45 | 0.05680 | 0.000991 | 146.37 | 0.2600 | 5.200 | 3.185 | 4.66 | 74% |
| | | 34.54 | 0.04470 | 0.000780 | 186.04 | 0.2594 | 5.187 | 3.177 | 2.89 | |
| ZnO:GO | | 34.41 | 0.04790 | 0.000836 | 173.55 | 0.2603 | 5.206 | 3.188 | 3.31 | 82% |
| | | 34.5 | 0.03630 | 0.000634 | 229.07 | 0.2597 | 5.193 | 3.180 | 1.9 | |
| ZnO:GO | | 34.44 | 0.05156 | 0.000900 | 161.25 | 0.2601 | 5.202 | 3.186 | 3.8 | 52% |
| 1 kV | | 34.53 | 0.04920 | 0.000859 | 169.02 | 0.2594 | 5.188 | 3.177 | 3.5 | |
| ZnO:GO | | 34.39 | 0.05810 | 0.001014 | 143.08 | 0.2605 | 5.209 | 3.190 | 4.88 | 75% |
| 1 kV (-) | | 34.48 | 0.04770 | 0.000833 | 174.31 | 0.2598 | 5.196 | 3.182 | 3.29 | |

The structural characteristics, such as interplanar spacing $d_{(002)}$ and lattice parameters *c*, were calculated using equations (2) and (3). Since the peak was highly dominantly of the (002) plane, the lattice parameters *a* was determined using the ratio between *c* and *a*, (*c*/*a*) = 1.633, that specific value of ZnO hexagonal wurtzite structure [32]. The dislocation density ($\delta$) represents the number of defect states as dislocation lines in the crystallite grain (nm$^{-2}$). The dislocation density was calculated using equation (4). The crystal defects per unit area increased as the crystal size gets smaller. This result was consistent with the DOC value, where the crystal with the smallest dislocation density of 5.21 ×10$^{-5}$ nm$^{-2}$ had the highest degree of crystallinity (82%).

$$\frac{1}{d^2_{(hkl)}} = \frac{4}{3}\left(\frac{h^2+hk+k^2}{a^2}\right) + \frac{l^2}{c^2} \quad (2)$$

$$c = \frac{\lambda}{\sin\theta} \quad (3)$$

$$\delta = \frac{1}{D^2} \quad (4)$$

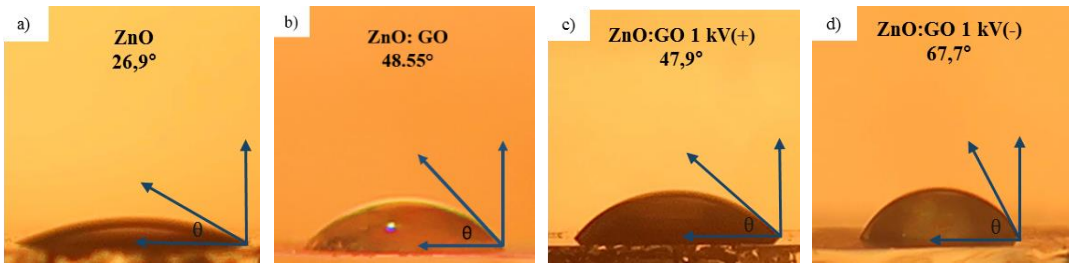


(a) (b) (c) (d)

**Figure 8**. The Results of ZnO:GO Submicron-Rods Samples Measurement using Contact Angle on Samples a) ZnO Non-Electric Field, b) ZnO:GO Non-Electric Field, c) ZnO:GO 1 kV (+), and d) ZnO:GO 1 kV (-)

**Structure Properties**

The SEM result showed that all samples had hexagonal morphology with a specific size on each diameter. This condition could be affecting the wetting properties of the surface samples. The wetting characteristics of each sample surface were determined by measuring the contact angle. The high-resolution camera captured the water droplets on the surface, allowing us to observe and measure the angle between the solid and liquid surfaces. If the contact angle is >90°, the sample surface is hydrophobic, whereas if <90°, the surface is considered hydrophilic [33]. Based on the picture in Figure 8, the contact angle of ZnO was 26.9°, ZnO:GO was 48.55°, ZnO:GO 1 kV (+) was 47.9°, and ZnO:GO 1 kV (-) was 67.7°. The contact angle increased with the raising of the rods' aspect ratio. The higher aspect ratio has lower surface density due to the surface topography [34]. The surface properties tended to be hydrophilic due to the high surface density of ZnO submicron-rods. This measurement showed that all samples of ZnO and ZnO:GO submicron-rods layer had good favorable interactions with the liquid on its surface.

The research primarily investigated the impact on crystal formation and morphology, and further studies may be needed to assess the electrical and optical properties of the ZnO:GO layers under different growth conditions. The study focused on a specific set of experimental conditions, such as the use of specific precursor materials and dopants, which may limit the generalizability of the results to different fabrication methods or compositions. Additionally, the application of an external electric field was explored only within a certain voltage range (±1 kV), and the potential effects of higher or lower voltages remain unexplored. The implications of this research are prominent for optoelectronics and nanomaterials. The controlled growth of ZnO:GO nanostructures with enhanced aspect ratios provides possibilities for optimizing device performances in optoelectronic applications. Future research in this area could explore diverse combinations of materials, alternative growth methods, and extended voltage ranges to further enhance the versatility and applicability of ZnO:GO nanostructures in optoelectronic devices.

## CONCLUSION

ZnO:GO submicron-rods have been successfully synthesized using the sol-gel method (self-assembly) with the addition of an external electric field. A different voltage between two cooper plates of ± 1 kV was set up to induce the external electric field around the systems. Applying an external field during self-assembly accelerated the ZnO hexagonal wurtzite crystal formation in a vertical growth direction. Fast crystal growth affects the crystals' quality and enhances the

dislocation density. The direction of the applied external field affected the structure and morphology of the ZnO rods. A negative external field induced a relatively smaller rod size distribution, making the aspect ratio larger. However, the degree of crystallinity (DOC) was increased by adding GO compounds without applying an external field. Adding GO compounds to the growth solution caused an increment in oxygen and hydroxyl groups, which reacted with $Zn^{2+}$ and subsequently formed a ZnO crystal. The carbon element from the graphene oxide compound seemed to attach to the prismatic plane of ZnO rods and bonded with the oxygen in the sublattice. The surfaces of ZnO and ZnO:GO sub-micron rods were hydrophilic, which was related to the topography of the resulting layer. Incorporation of an external field could generally conduct the well-organized ZnO and ZnO:GO rods alignment.

## ACKNOWLEDGMENT

The authors would like to acknowledge to Universitas Padjadjaran for financial supporting under project of Hibah Riset Unpad contract no.1549/UN6.3.1/PT. 00/2023.

## AUTHOR CONTRIBUTIONS

Annisa Nur Rahmawati: Methodology, Validation, Investigation, Resources, and Writing - Original Draft; Nabilah Putri Utami: Methodology, Resources; Lusi Safriani: Formal Analysis, Data Curation; Ayi Bahtiar: Validation, Investigation, Writing - Review & Editing; Wa Ode Sukmawati Arsyad: Formal Analysis, Writing - Review & Editing; Euis Siti Nurazizah: Resources; Annisa Aprilia: Conceptualization, Methodology, Resources, Writing - Original Draft, Supervision

## DECLARATION OF COMPETING INTEREST

The authors declare that they have no known competing financial interests or personal relationships that could have appeared to influence the work reported in this paper.

## REFERENCES

[1] Borysiewicz MA. ZnO as a Functional Material, A Review. *Crystals*. 2019; 9(10): 1-29. DOI: https://doi.org/10.3390/cryst9100505

[2] Singh AK and Singh SK. Optical Properties of ZnO. *Metal Oxides: Nanostructured Zinc Oxide*. Elsevier; 2021; 189-208. DOI: https://doi.org/10.1016/B978-0-12-818900-9.00014-0

[3] Nahhas AM. Recent Advances of ZnO Based Nanowires and Nanorods Devices. *American Journal of Nanomaterials*. 2018; 6(1): 15-23. DOI: https://doi.org/10.12691/ajn-6-1-2

[4] Basher MK, Shah Riyadh SM, Hossain MK., Hassan M, Akand Rafiq MdA, Amir Al-Zumahi SM, Abdul Matin Md, Das N, Nur-E-Alam M. Development of Zinc-Oxide Nanorods on Chemically Etched Zinc Plates Suitable for High-Efficiency Photovoltaic Solar Cell. *Optical and Quantum Electronics.* 2023; 55: 322. DOI: https://doi.org/10.1007/s11082-022-04474-1

[5] Zhou J, Qiao Q, Tan Y, Wu C, Hu J, Qiu X, Wu S, Zheng J, Zhang C, Xuan Yu, Xiaoming Yu, and Li Z. The Improvement of Polymer Detector Based on 1D-ZnO Nanorod Arrays/0D-ZnO Quantum Dots Composite Film. *Optical Material.* 2023; 142: 114086. DOI: https://doi.org/10.1016/j.optmat.2023.114086

[6] Mishra S, Przezdziecka E, Wozniak W, Adhikari A, Jakiela R, Paszkowicz W, Sulich A, Ozga M, Kopalko K, Guziewicz E. Structural Properties of Thin ZnO Films Deposited by ALD under O-Rich and Zn-Rich Growth Conditions and Their Relationship with Electrical

Parameters. *Materials*. 2021; 14(14): 4048. DOI: https://doi.org/10.3390/ma14144048

[7] Anh Thi Le, Ahmadipour M, Swee-Yong Pung, A Review on ZnO-based Piezoelectric Nanogenerators: Synthesis, Characterization Techniques, Performance Enhancement and Applications. *Journal of Alloy Compounds*. 2020; 156172. DOI: https://doi.org/10.1016/j.jallcom.2020.156172

[8] Ahmad T, Pandey V, Husain MS, Adiba, Munjal S. Structural and Spectroscopic Analysis of Pure Phase Hexagonal Wurtzite ZnO Nanoparticles Synthesized by Sol-gel. *Materials Today: Proceedings*. 2022; 49: 1694-1697. DOI: https://doi.org/10.1016/j.matpr.2021.07.456

[9] Wang ZL, and Song J. Piezoelectric Nanogenerators Based on Zinc Oxide Nanowire Arrays. *Science.* 2006; 312 (5771): 242–246. DOI: https://doi.org/10.1126/science.1124005

[10] Tripathi P, Nayak SK, Tripathi GS. Electronic Structure Theory of Strained Wurtzite ZnO. *Physica Scripta*. 2020; 95(12): 125801. DOI: https://doi.org/10.1088/1402-4896/abc118

[11] Consonni V, and Lord AM. Polarity in ZnO Nanowires: A Critical Issues Piezotronics and Piezoelectric Devices. *Nano Energy*. 2021; 83: 105789. DOI: https://doi.org/10.1016/j.nanoen.2021.105789

[12] Aprilia A, Fernando H, Bahtiar A, Safriani L, Hidayat R. Influences of Al Dopant Atoms to the Structure and Morphology of Al Doped ZnO Nanorod Thin Film. *Journal of Physic Conference Series*. 2018; 1080: 012009. DOI: https://doi.org/10.1088/1742-6596/1080/1/012009

[13] Avcı B, Caglar Y, and Caglar M. Controlling of Surface Morphology of ZnO Nanopowders via Precursor Material and Al Doping. *Materials Science in Semiconductor Processing*. 2019; 99: 149-158. DOI: https://doi.org/10.1016/j.mssp.2019.04.028

[14] Rabia A, Riaz A, Naveed A, Mubarik, and Ehtesham F. Effect of Structure Modifying Agents on the Structural, Morphological and Optical Features of Hydrothermally Grown ZnO. *Journal of Nanoscience and Nanotechnology*. 2020; 20(5): 3265-3273. DOI: https://doi.org/10.1166/jnn.2020.17389

[15] Wang J, Chen R, Xiang L, Komarneni S. Synthesis, Properties and Applications of ZnO Nanomaterials with Oxygen Vacancies: A Review. *Ceramics International*. 2018; 44(7): 7357-7377. DOI: https://doi.org/10.1016/j.ceramint.2018.02.013

[16] Liu WM, Li J, and Zhang HY. Reduced Graphene Oxide Modified Zinc Oxide Composites Synergistic Photocatalytic Activity under Visible Light Irradiation. *Optik*, 2020; 207. DOI: https://doi.org/10.1016/j.ijleo.2019.163778

[17] Majumder P and Gangopadhyay R. Evolution of Graphene Oxide (GO)-based Nanohybrid Materials with Diverse Compositions: An Overview. *Royal Society of Chemistry Advances*. 2022; 9: 5686–5719. DOI: https://doi.org/10.1039/D1RA06731A

[18] Shahzad S, Javed S, and Usman M. A Review on Synthesis and Optoelectronic Applications of Nanostructured ZnO. *Frontiers in Materials*. 2021; 8. DOI: https://doi.org/10.3389/fmats.2021.613825

[19] Prijamboedi B, Maryanti E, and Haryati T. Preparation of Vertically Aligned ZnO Crystal Rods in Aqueous Solution at External Electric Field. *Materials Science-Poland*. 2014; 32(2): 157–163. DOI: https://doi.org/10.2478/s13536-013-0191-8.

[20] Ching KL, Li G, Ho YL, and Kwok HS. The Role of Polarity and Surface Energy in the Growth Mechanism of ZnO from Nanorods to Nanotubes. *Crystall Engineering Comm* 2016; 18(5): 2219-2224. DOI: https://doi:10.1039/C5CE02164B.

[21] Utami NP, Rahmawati AN, Bahtiar A, Suryaningsih S, and Aprilia A. Synthesis of ZnO Submicron-Rods by Self Assembly Method and Its Properties. *AIP Conference Proceeding.* 2023; 2604; 020024. DOI: https://doi.org/10.1063/5.0114479.

[22] Kashyap S, Mishra S, and Behera SK. Aqueous Colloidal Stability of Graphene Oxide and Chemically Converted Graphene. *Journal of Nanoparticles*. 2014; 1–6. DOI: https://doi.org/10.1155/2014/640281

[23] Molefe FV, Mofokeng SJ, Khenfouch M, Achehboune M, Dhlamini MS, Mothudi BM, Koao LF. The Effect of Zn2+ on the Anion Vacancies in ZnO Thin-films Grown using Chemical Bath Deposition. *Journal of Physics Conference Series*. 2019; 1292: 012016 DOI: https://doi.org/10.1088/1742-6596/1292/1/012016

[24] Pérez LAMP, Cepeda ABM, Alamilla RC, Armenta JLR, and Valdéz SS. Nanostructures of Graphene Oxide Modified with ZnO: Synthesis and Photocatalyst Evaluation under Sunlight. *Fullerenes Nanotubes Carbon Nanostructure*. 2019: 27(8): 632-639. DOI: https://doi.org/10.1080/1536383x.2019.1627522

[25] Song Y, Zhang S, Zhang C, Yang Y, and Lv K. Raman Spectra and Microstructure of Zinc Oxide Irradiated with Swift Heavy Ion. *Crystals*. 2019; 9(8): 395. DOI: https://doi.org/10.3390/cryst9080395.

[26] Shukla V and Patel AJ. Effect of Doping Concentration on Optical and Electrical Properties of Intrinsic N-type ZnO (i-ZnO) and (Cu, Na and K) Doped p-type ZnO Thin Films Grown by Chemical Bath Deposition Method. *Nanosystems: Physics, Chemistry, Mathematics.* 2020; 11(4): 391-400. DOI: https://doi.org/10.17586/2220-8054-2020-11-4-391-400.

[27] Ahmed G, Hanif M, Mahmood K, Yao R, Ning H, Jiao D, Wu M, Khan J, and Liu Z. Lattice Defects of ZnO and Hybrids with GO: Characterization, EPR and Optoelectronic Properties. *AIP Advances. 2018*; 8(2): 025218. DOI: https://doi.org/10.1063/1.5011356

[28] Akbari E, Akbari I, and Ebrahimi M. sp2/sp3 Bonding Ratio Dependence of the Band-gap in Graphene Oxide. *The European Physical Journal B*. 2019; 92: 1-6. DOI: https://doi.org/10.1140/epjb/e2019-90675-y

[29] Mustapha S, Ndamitso MM, Abdulkareem AS, Tijani JO, Shuaib DT, Mohammed AK, and Sumaila A. Comparative Study of Crystallite Size Using Williamson-Hall and Debye-Scherrer Plots for ZnO Nanoparticles. *Advances in Natural Science: Nanoscience and Nanotechnology*. 2019; 10(4): 045013. DOI: https//doi.org/10.1088/2043-6254/ab52f7

[30] Londoño-Restrepo SM, Jeronimo-Cruz R, Millán-Malo BM, Rivera-Muñoz EM, and Rodriguez-García ME. Effect of the Nano Crystal Size on the X-ray Diffraction Patterns of Biogenic Hydroxyapatite from Human, Bovine, and Porcine Bones. *Scientific Reports*. 2019; 9: 5915. DOI: https//doi.org/10.1038/s41598-019-42269-9

[31] Abdulrahman AF, Ahmed SM, Hamad SM, Almessiere MA, Ahmed NM, and Sajadi SM. Effect of Different pH Values on Growth Solutions for the ZnO Nanostructures. *Chinese Journal of Physics*. 2021; 71: 175-189. DOI: https//doi.org/10.1016/j.cjph.2021.02.013

[32] Ghosh S, Gosh A, Pramanik Z, Kuiri KP, Sen R, and Neogi SK. Synthesis of ZnO Nanoparticles by Co-precipitation Technique and Characterize the Structural and Optical Properties of These Nanoparticles. *Journal of Physics Conference Series*. 2022. 2349; 012014. DOI: https//doi.org/ 10.1088/1742-6596/2349/1/012014

[33] Hebbar RS, Isloor A, and Ismail AF. Contact Angle Measurement. *Membrane Characterization*. (2017): 219-255. DOI: https//doi.org/ 10.1016/b978-0-444-63776-5.00012-7

[34] Ellinas K, Dimitrakellis P, Sarkiris P, and Gogolides E. A Review of Fabrication Methods, Properties and Applications of Superhydrophobic Metals. *Processes*. 2021; 9(4): 666. DOI: https://doi.org/10.3390/pr9040666